Rheological Behaviour of Single–phase non-Newtonian Polymer Solution in Complex Pore Geometry: A Simulation Approach

P.E.G. Idahosa*[1], G.F. Oluyemi[2], M. B. Oyeneyin[2], and R. Prabhu[2].
[1] IDEAS Research Institute, Robert Gordon University, Riverside East, Garthdee Road, Aberdeen, AB10 7GJ, United Kingdom.
[2] School of Engineering, Robert Gordon University, Riverside East, Garthdee Road, Aberdeen, AB10 7GJ, United Kingdom.
Address all correspondence to: P.E.G. Idahosa, IDEAS Research Institute, Robert Gordon University, Riverside East, Garthdee Road, Aberdeen, AB10 7GJ, United Kingdom. Tel: +44 (0) 1224262451, E-mail: p.e.g.idahosa@rgu.ac.uk*

Abstract: **One of the most important criteria for evaluating chemical enhanced oil recovery (EOR) processes that use polymers is its rheological behaviour which in turn account for other physical effects of adsorption and resistance factors during polymer-formation rock interactions. However, complete knowledge of behaviour of polymer solution in porous media has not yet been fully gained. A computational fluid dynamics (CFD) simulations implemented in COMSOL Multiphysics is used to simulate a 1-D single-phase, non-elastic xanthan gum flow in geometries approximating formation pore throats. Simulation results show the degree of solution viscosity degradation at different inlet pressures and shear rates at varying pore constriction diameters. Results also show that numerical techniques can predict the performances of polymer solution applications in actual field operational conditions and aid in design and interpretation of laboratory tests.**

Keywords: **rheological behaviour, pore-throats, xanthan gum, pressure distribution, injection rates.**

1. Introduction

Polymers are used for a variety of applications in the oil and gas industry including drilling mud viscosity modification [1], Filtration Loss Control [2, 3], Enhanced oil Recovery (EOR) [4], chemical placement [5], sand control [6], etc. The selection of appropriate polymers for drilling or EOR is based on operational efficiency, costs and economics. Chemicals are expensive on a unit basis; therefore, the quantity of polymer economically sacrificed for incremental reservoir crude oil recovery is of priority concern for a practical EOR project.

Rheology is one most important attribute of polymers. Therefore, accurate computation of polymer rheological behaviour in porous media is considered as an important aspect for accurate well pressure representation, pressure distribution [7] far away from the wellbore and accurate predictions of injection rates since the economics are quite sensitive to rates of injection. Viscous dispersion is assumed to be localised only in the pore throats while grain size determines the spacing between pore throats [8]. As the viscosity of non-Newtonian polymer solution depends on shear rate, shear rate calculations must be accurate.

Polymers exhibit extremely complex rheological behaviour during flow in porous media [**9**]. This behaviour depends on the nature of the pore structure of the porous media and polymer system itself [10], as well as the interaction between the components in the polymer and the porous media [9, 11]. In the field, partially hydrolysed polyacrylamides (HPAM) and xanthan gums are commercially used in EOR processes [4, 12**,** 13]. It is, however, believed that both polymers give unsatisfying performances [12]. For instance, effective polymers for high salinity environments are an issue. In furtherance to performance issues, it is desirable for a polymer solution to have a low pressure drop at injection wells to achieve higher injectivity and greater viscosity at low rates in the reservoirs to enhance sweep efficiency. However, the displacement efficiency of polymer solution is affected by shear-thinning behaviour, particularly on a pore scale. Xanthan gum exhibits shear-thinning or viscous behaviour while HPAM exhibits both viscous and elastic characteristics [14, 15]. Therefore, a large amount of research efforts has

been devoted to gaining a better understanding of polymer flow behaviour in porous media in the past recent years. Inspite of these efforts, several issues have been only partially resolved [10].

Several authors have concentrated their research focus on investigating (single-phase) viscoelastic fluids experimentally and numerically in both porous media and constrictions representative of pores [7, 12, 16-19]. It has also been argued that apparent viscosity of polymers decreases with pore size [20]. In this study, a computational fluid dynamics (CFD) simulations implemented in COMSOL multiphysics interface is used to simulate a 1-D single-phase, non-elastic xanthan gum flow in geometries approximating pore throats. The goal of this work is not only predictive in nature, but also to obtain a better fundamental understanding of the physics of viscous fluid dynamics at the pore-constriction level.

2. Mathematical and Numerical Framework

2.1 Model Definition

Xanthan molecules can be approximated as "rigid rod"; therefore, its dilatant effect during flow in porous medium is negligible [15]. For this reason, it is more suitable for simulation studies since it can be assumed that xanthan solution exhibits only viscous or shear-dependent viscosity. In the model, a Comsol iterative approach was used to solve the pressure field because the pressure depends on the aqueous phase viscosity which for non-Newtonian fluids is a function of shear rates and the pressure itself. The momentum and continuity equations are those that govern the velocity and pressure of an incompressible fluid [21]. For complex pore throat geometries (such as the type considered in this study), these equations are impossible to solve analytically, and hence numerical method such as the finite element method (FEM) must be implemented. For non-Newtonian flow therefore, the equations to solve are the momentum and continuity equations:

$$\rho\frac{\partial \boldsymbol{u}}{\partial t}-\nabla.\mu\left(\nabla \boldsymbol{u}+(\nabla \boldsymbol{u})^{T}\right)+\rho \boldsymbol{u}.\nabla \boldsymbol{u}+\nabla p=0 \qquad \text{(Eq. 1)}$$

$$\nabla.\,\boldsymbol{u}=0 \qquad \text{(Eq. 2)}$$

Where, μ = viscosity (kg/(m.s)), ρ = fluid density (kg/m^3), $(\nabla u)^T$ = shear effects which describe viscous forces and the extra stress contribution from the polymer, p = pressure (Pa), u = velocity (m/s), ∇ = del operator.

To account for polymers' viscous or thinning behaviour, we chose to use the Carreau model (Eq. 3) [22] for the problem because it covers and combines the power-law region and the two Newtonian regions of the viscosity curve.

$$\mu_{sh}=\mu_{\infty}+(\mu_p^0-\mu_{\infty})[1+(\lambda\dot{\gamma}_{eff})^2]^{(n-1)/2} \qquad \text{(Eq. 3)}$$

Where, μ_{sh} = apparent shear viscosity in porous media, μ_p^0 = polymer viscosity at zero shear rate, μ_∞ = μ_w = viscosity at infinite shear rate, λ = time constant (i.e. relaxation time for realignment of polymer rods in a shear flow field) is found from bulk viscosity measurements, $\dot{\gamma}_{eff}$ = rate of deformation (also called effective shear rate in a shear flow), n = dimensionless constant known as the shear-thinning index that depends on the polymer concentration. $0.4 \le n \le 1$ for pseudoplastic or shear-thinning fluids.

For an axisymmetry model (discussed in the following section), the shear rate in Carreau equation is written in cylindrical coordinates as (Eq. 4):

$$\dot{\gamma}=\sqrt{\frac{1}{2}\left((2u_r)^2+2(u_z+v_r)^2+(2v_z)^2+4(\frac{u}{r})^2\right)} \qquad \text{(Eq. 4)}$$

where u, v are velocity vectors, and in particular,

$$\breve{p}(r,0,z)=p(r,z) \qquad \text{(Eq. 5)}$$

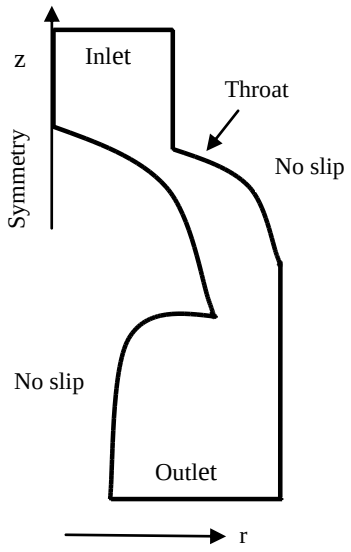

Fig. 1. Pore throat geometry model used for the simulation

$$\breve{u}(r,0,z) = u(r,z) \qquad \text{(Eq. 6)}$$

and

$$u = (u_r, u_z) \qquad \text{(Eq. 7)}$$

2.2 Model Geometrical Domain

The model geometry is shown in fig. 1. The figure shows the modelling interest in the region of contraction (throat) and expansion with different cross-sectional areas. However, the effects at the inlet and outlet regions with different cross-sectional areas are also evaluated. To reduce the computational efforts without affecting the model dimension, the domain, the initial and the boundary conditions and other body forces are approximated as symmetric with respect to a straight line (fig. 1). In this case, the flow can be modelled by the 3-D axisymmetric Stokes or Navier-Stokes equations which take advantage of the hypothesis of symmetry [23]. The axisymmetric model, in particular, is also easily coupled with an axisymmetric 1-D model [24]. Therefore, we use the axisymmetric 2-D model to reproduce a 3-D effect in the region of interest where there is pore contraction-and-expansion as shown in the geometry (fig. 1). This reduces the size of the problem without losing the 3-D features and without any assumption on the velocity profile.

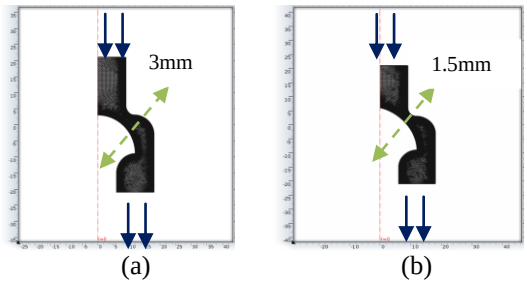

Fig. 2. Model simulation geometries and mesh arrangements: (a) 3mm pore throat (b) 1.5mm pore throat.

2.2.1 Constriction (Pore Throat) Geometry Used for the Simulation

Figure 2 shows the dimensions of the pore constriction used in the simulation. Though the geometry is hypothetical, it however provides the insight needed for understanding the fundamental physics underlying fluid behaviour at the diverging-converging flows mimicking natural reservoir porous systems. The geometry has varying cross-section perpendicular to flow direction. The number of elements and mesh configurations differ for the different cases as discussed under results and discussions section.

2.3 Boundary Condition Settings

2.3.1 Pressure outlet

Equations 5 through 7 imply that for an axisymmetric flow, the pressure, P and the cylindrical velocity components, u_r, u_θ, u_z are independent of the angular variable θ with unknown (**u**, p), $\boldsymbol{u} = (u_r, u_z)$; where z and r are symmetry directions. We use the Dirichlet boundary condition (BC) form for the momentum and extra stress application modes; while the Neumann BC form was used for the pressure outlet condition [21] since application of the Neumann form to the momentum application mode enforces the pressure out boundary condition equal zero (Eq. 8). Therefore, inlet and outlet boundary conditions are given and set to fixed pressures (Eq. 8) and vanishing viscous stresses (Eq. 9):

$$\left.\begin{aligned} p &= p_{in} \\ p &= 0 \end{aligned}\right\} \qquad \text{(Eq. 8)}$$

and

$$\boldsymbol{n}.[\eta(\nabla \boldsymbol{u} + (\nabla \boldsymbol{u})^T)] = 0 \qquad \text{(Eq. 9)}$$

where n is the boundary unit normal vector.

2.3.2 Slip or Axial Symmetry Boundary Condition

Due to the axisymmetric nature of the geometry, a symmetry BC at r=0 is used since one half of the domain is modelled (fig. 1). The rotational axial symmetry condition (as expressed by Eq.10) is described as zero flow normal to the boundary.

$$\boldsymbol{u}.\boldsymbol{n} = 0 \qquad \text{(Eq. 10)}$$

2.3.3 Wall Boundary Condition

The wall effect (i.e. fluid velocity is zero at a wall) imposes the no-slip boundary condition at the wall which justifies setting the normal component of the boundary stress contribution from the polymer equal to zero (Eq. 11):

$$\boldsymbol{u} = 0 \qquad \text{(Eq. 11)}$$

2.4 Numerical Solution of Axisymmetric flow

Let Ω be the 2-D half section of the axisymmetric 3-D domain $\breve{\Omega}$ under consideration as shown in fig. 1 and V and Q are weighted Sobolev spaces (recall that: a Sobolev space is a space of functions with sufficiently many derivatives for some application domain, such as partial differential equation and equipped with a norm that measures both the size and regularity of a function) [23]. Assume the data are axisymmetric with zero angular component. The axisymmetric Stokes problem is: Find

$(\boldsymbol{u}, p), \boldsymbol{u} = (u_r, u_z)$, *in V x Q such that*

$$\begin{cases} v\int_\Omega (\nabla u : \nabla v) r dx + v\int_\Omega u_r v_r \frac{1}{r} dx \\ -\int_\Omega (div\, v)\, p\, r dx - \int_\Omega v_r\, p\, dx = \int_\Omega f.v r dx \\ -\int_\Omega (div\, u)\, q\, r dx = \int_\Omega u_r\, q dx = 0 \end{cases} \qquad (Eq.12)$$

for all (v, q) in V x Q.

To recover the 3-D solution $(\breve{u}, \breve{p})$ from (u, p), the 3-D domain $\breve{\Omega}$ is described in cylindrical coordinates (r, θ, z). Then (Eq. 13)

$$\breve{u}(r,\theta,z) = \begin{pmatrix} \breve{u}_x \\ \breve{u}_y \\ \breve{u}_z \end{pmatrix} = \begin{pmatrix} u_r(r,z)\cos\theta \\ u_r(r,z)\sin\theta \\ u_z(r,x) \end{pmatrix} \qquad \text{(Eq. 13)}$$

and

$$\breve{p}(r,\theta,z) = p(r,z). \qquad \text{(Eq. 14)}$$

The model simulation input parameter for 2500ppm Xanthan gum is shown in table 1 [25].

3. Results and Discussion

3.1 Comparative Analysis of the Effects of Different Constrictions and Inlet Pressures on Viscosity.

Figure 2 shows the mesh arrangements of the pore constrictions on which the simulations were performed. Due to the challenging nature of fluid behaviour in such constrictions, the required mesh is extra fine. Mesh sensitivity analysis was carried out to establish mesh arrangements and/or refinements. This was done to ensure that

Table I. Simulation input values

Parameter	μ_∞ (Pa.s)	μ_p^0 (Pa.s)	n	λ (s)	P (kg/m^3)
Value	0.0015	11.6	0.38	0.01	500

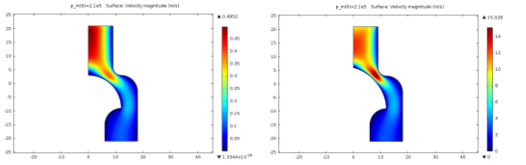

(a) (b)

Fig. 3. Model domain velocity field: (a) 3mm constriction, (b) 1.5mm constriction.

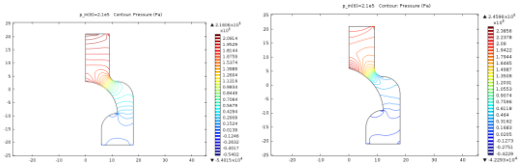

(a) (b)

Fig. 4. Pressure distribution contour: (a) 3mm constriction, (b) 1.5mm constriction.

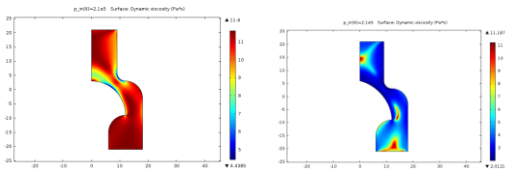

(a) (b)

Fig. 5. Model domain viscosity profile: (a) 3mm constriction, (b) 1.5mm constriction.

the solution is not affected by further mesh refinements. Figure 2a (3mm pore throat) has 20827 elements and mesh area of 395.4mm^2 with an average quality of 90.41%. While fig. 2b (1.5mm throat) has 20923 elements and mesh area of 377.4mm^2 with an average quality of 90.45%. It is therefore believed that no further refinement is required for a better solution to the problem.

Figure 3 compares the velocity field of the non-Newtonian xanthan fluid for the different pore throats (3mm and 1.5mm). Due to the outlet greater cross-section, there is a higher velocity distribution at the inlet compared to the outlet. Interestingly, the figure also shows that the greatest velocity gradient and shear rates occur at the centre of the constriction compared to the near wall due to the no-slip boundary conditions imposed. This higher velocity distribution at the centre is however more pronounced in 3b compared to 3a due to its reduced contraction.

Notably, fig. 4 shows that the contours are smooth in the vicinity of the constriction. The

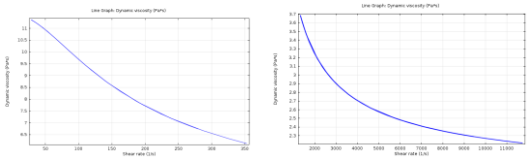

(a) (b)

Fig. 6. Effects of varying shear rates on viscosity: (a) 3mm constriction, (b) 1.5mm constriction.

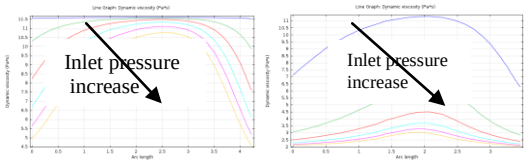

(a) (b)

Fig. 7. Pressure gradient effects on viscosity: (a) 3mm constriction, (b) 1.5mm constriction.

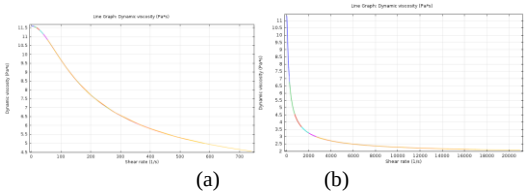

(a) (b)

Fig. 8. Effects on viscosity of different shear rates for all inlet pressures: (a) 3mm constriction, (b) 1.5mm constriction. For fig. (a), onset of shear-thinning is at about 10^{-s}. Fig. (b) suggests premature shear-thinning xanthan fluid behaviour induced by shear pre-deformation resulting from reduced pore constriction.

figure shows the magnitude or rate of change of the pressure parameters. Therefore, the smoother the contours (fig. 4b), the faster the change in the pressure difference parameter across the constriction compared to fig. 4a. Hence, the higher pressure drop at the constriction induces a greater velocity at that point which in turn causes severe viscosity degradation in fig. 5b compared to fig. 5a. The plausible explanation for this is that, at a wall, fluid velocity is zero; hence polymers are unable to exert a force on the wall as no polymer can span the wall boundary. Figure 5b therefore suggests premature shear-thinning behaviour induced by shear pre-deformation resulting from the reduced (*1.5mm*) constriction.

As the xanthan fluid is shear-thinning, its viscosity is a function of shear rates (fig. 6). Compared to fig. 6a for the same inlet pressure of 10 KPa, the reduced throat (fig. 6b) causes a resultant increase in shear rates which

consequently decreases the xanthan fluid viscosity from about 11.5 Pa*s to about 6.33 Pa*s.

Figure 7 shows the effects of increasing inlet pressures (and pressure gradients) on viscosity across the throat. The figure shows that the greater the inlet pressure, the more the velocity gradient and shear rates; and the more the viscosity is degraded across the constriction. The viscosity degradation is more evident in fig. 7b compared to fig. 7a.

Figure 8 further emphasizes the effects of shear rates on viscosity for all pressures. Figure 8a shows that the onset of shear-thinning is at about 10^{-s}; while fig. 8b suggests premature and excessive shear-thinning behaviour induced by shear pre-deformation resulting from the reduced (1.5mm) pore constriction.

8. Conclusions

Numerical simulations were performed using Comsol Multiphysics 4.3a software to solve a coupled momentum and continuity equations for the purpose of studying the dynamic rheological behaviour of non-elastic xanthan gum polymer solution in porous media contraction-and-expansion geometries approximating pore throats. Results showed that the Carreau equation sufficiently described the viscosity behaviour of the solution at the pore constriction. As the pore throat decreases, the solution viscosity drastically reduces. Also, the greater the inlet pressure, the more the velocity gradient and shear rates; and the more the viscosity is degraded across the constriction. Furthermore, CFD simulations showed that shear-thinning behaviour can affect the solution displacement efficiency. Finally, this study offers the possibility for reliable prediction of the rheological behaviour of non-elastic, non-Newtonian fluid such as xanthan gum in porous media, and the design and interpretation of laboratory tests including the predictions of the performances of polymer solution applications in actual field conditions.

9. References

[1] R. Navarrete, H. Dearing, V. Constien, K. Marsaglia, J. Seheult, and P. Rodgers, "Experiments in Fluid Loss and Formation Damage with Xanthan-Based Fluids While Drilling," *IADC/SPE Asia Pacific Drilling Technology. Kuala Lumpur, Malaysia, 11-13 September, 2000.*

[2] P.E. Clark, "Analysis of fluid loss data II: Models for dynamic fluid loss," *Journal of Petroleum Science and Engineering.* 2010; 70(3):191-197.

[3] R. Navarrete, R. Himes, and J. Seheult, "Applications of Xanthan Gum in Fluid-Loss Control and Related Formation Damage," paper SPE 59535 presented at the SPE Permian Basin Oil and Gas Recovery Conference. *Midland, TX, Mar.* 21-23, 2000.

[4] J. Wang, and M. Dong, "Optimum effective viscosity of polymer solution for improving heavy oil recovery," *Journal of Petroleum Science and Engineering.* 2009; 67(3):155-158.

[5] K. Taylor and H. Nasr-El-Din, "Coreflood evaluation of in-situ gelled acids. *International Symposium and Exhibition on Formation Damage Control*," 2002.

[6] L. Zhang, S. Deng, and M. Huang, "Cationized polyacrylamides AEE for use as clay stabilizer/sand controller," *Oilfield Chem.* 2002; 19:208-209.

[7] J. Aguayo, H. Tamaddon-Jahromi, and M. Webster, "Excess pressure-drop estimation in contraction and expansion flows for constant shear-viscosity, extension strain-hardening fluids," *Journal of Non-Newtonian Fluid Mechanics",* 2008; 153(2):157-176.

[8] G. Chauveteau," The Grain and Pore Throat Model: A Tool to Predict Mass Transport and Formation Damage," *SPE Int. Symp. on Formation Damage Control, Lafayette, Louisiana*; 2002. p. 20-21.

[9] [L, Cheng, P. Lian, and R. Cao, "A Viscoelastic Polymer Flooding Model Considering the Effects of Shear Rate on Viscosity and Permeability," *Petroleum Science and Technology.* 2013; 31(1):101-111.

[10] P. Zitha, "Prediction of Polymer Viscosity Reduction in Pores Using an Exact Depletion Profile," *SPE European Formation Damage Conference*; 2001.

[11] S. Yuan, D. Han, Q. Wang and H. Yang, "Numerical simulator for the combination process of profile control and polymer flooding," *International Oil and Gas Conference and Exhibition in Beijing, China*; 2000.

[12] P. Zhang, Y. Wang, Y. Yang, J. Zhang, X. Cao, and W. Chen, "One Factor Influencing the Oil-displacement Ability of Polymer Flooding: Apparent Viscosity or Effective Viscosity in Porous Media?" *Petroleum Science and Technology.* 2012; 30(14):1424-1432.

[13] A. Afsharpoor, M.T. Balhoff, R. Bonnecaze, and C. Huh, "CFD modeling of the effect of polymer elasticity on residual oil saturation at the pore-scale," *Journal of Petroleum Science and Engineering.* 2012; 94-95:79-88.

[14] A. Alsofi, and M. Blunt," Streamline-based simulation of non-Newtonian polymer flooding," *SPE Journal.* 2010; 15(4):895-905.

[15] A. Al-Sofi, T. La Force and M. Blunt, "Sweep Impairment Due to Polymers Shear Thinning," *SPE Middle East Oil and Gas Show and Conference; March 15-18,* 2009.

[16] L. Cheng, R. Cao, "Constitutive model of viscous-elastic polymer solution in porous media," *Petroleum Science and Technology.* 2010; 28(11):1170-1177.

[17] D.M., Binding, P. Phillips, and T. Phillips, "Contraction/expansion flows: The pressure drop and related issues," *Journal of Non-Newtonian Fluid Mechanics.* 2006; 137(1):31-38.

[18] Y. Fan, R. Tanner, and N. Phan-Thien, "Galerkin/least-square finite-element methods for steady viscoelastic flow," *Journal of Non-Newtonian Fluid Mechanics.* 1999; 84(2):233-256.

[19] R. Bird, W.E. Stewart, and E.N. Lightfoot, "*Transport phenomena,"* 1960; pp. 56.

[20] G. Chauveteau, "Rodlike polymer solution flow through fine pores: influence of pore size on rheological behaviour," *Journal of Rheology.* 1982; 26:111.

[21] T.J. Craven, J.M. Rees and W.B. Zimmerman, "Stabilised finite element modelling of oldroyd-B viscoelastic flows," in *COMSOL Conference*; Birmingham, 2006.

[22] P.J. Carreau, "Rheological equations from molecular network theories," *Transactions of the Society of Rheology.* 1972; 16(1):99-127.

[23] C. Bernardi, M. Dauge, Y. Maday, and M. Azaıez, "Spectral Methods for Axisymmetric Domains, Series in Applied Mathematics 3," *Gauthier–Villars & North-Holland, Elsevier, Paris,* 1999.

[24] K. Lagana, G. Dubini, F. Migliavacca, R. Pietrabissa, G. Pennati, and A. Veneziani, "Multiscale modelling as a tool to prescribe realistic boundary conditions for the study of surgical procedures," *Biorheology.* 2002; 39(3):359-364.

[25] M. Escudier, I. Gouldson, A. Pereira, F. Pinho, and R. Poole, "On the reproducibility of the rheology of shear-thinning liquids," *Journal of Non-Newtonian Fluid Mechanics.* 2001; 97(2):99-124.

9. Acknowledgments

The authors gratefully acknowledge the Petroleum Technology Development Fund (PTDF), Nigeria for funding the PhD work from which results/ideas used in this paper were generated.